Conical versus Gaussian terahertz emission from two-color laser-induced air plasma filaments

Christian Buhl Sørensen, Christian Buhl Sørensen, Léo Guiramand, Jérôme Degert, Marc Tondusson, Esben Skovsen, Eric Freysz, Emmanuel Abraham

Conical vs Gaussian terahertz emission from two-color laser-induced air plasma filaments

CHRISTIAN BUHL SØRENSEN[1], LÉO GUIRAMAND[2], JÉRÔME DEGERT[2], MARC TONDUSSON[2], ESBEN SKOVSEN[1], ERIC FREYSZ[2], AND EMMANUEL ABRAHAM[2,*]

[1] *Department of Materials and Production, Aalborg University, Denmark*
[2] *Univ. Bordeaux, CNRS, LOMA, UMR 5798, F-33400 Talence, France*
[*] *Corresponding author: emmanuel.abraham@u-bordeaux.fr*

Compiled January 16, 2020

We demonstrate that the far-field terahertz beam generated from a Ti:Sapphire two-color laser-induced filament can exhibit a conical or Gaussian distribution depending on the filtering experimental conditions. Using both an incoherent Golay cell detector and a two-dimensional coherent electro-optic detection covering the 0.2-3 THz spectral range, in our experimental conditions, we provide evidences that the conical emission is due to photoinduced carriers in the silicon filter typically used to block the remaining pump laser light. Moreover, the terahertz beam retrieves an almost TEM_{00} Gaussian spatial distribution when the silicon filter is preceded by a large bandgap ceramic filter, which stops the pump beam preventing carriers generation in the silicon filter.

OCIS codes: (110.6795) Terahertz imaging; (300.6495) Spectroscopy, terahertz;(350.5400) Plasmas; (140.3295) Laser beam characterization.

http://dx.doi.org/10.1364/ao.XX.XXXXXX

Two-color laser-induced air plasma filaments is a very convenient mean to generate intense ultrashort terahertz (THz) pulses [1–4]. This THz emission has been described by different models such as two-dimensional (2D) transverse photocurrent [5], four-wave mixing [6], or a combination of the two as well. In short, within the plasma filament induced by a focused femtosecond millijoule optical pulse at a fundamental frequency ω and its second harmonic 2ω, electrons are accelerated in a step-like response with a frequency content much higher than the one subtended by the envelope of the femtosecond two-color electric laser field [7].

The method presents obvious advantages such as relative simplicity, self-repairing gas media and possibility of high excitation laser intensity. These benefits enable unique applications for broadband THz time-domain linear spectroscopy. Non-linear spectroscopy requires tight focusing and, consequently, a full spatial characterization of THz radiation emitted from the air filament is necessary. In 2006, using a scanning aperture and an electro-optic coherent detection, Zhong *et al.* first reported a THz beam profile with an interference structure caused by the phase walk-off between the THz and the optical radiation propagating inside the filament [3]. This off-axis phase-matched so-called "conical" THz emission has also been observed using incoherent detections [8–10]. To account for this conical THz emission and considering the relative phase change between the two-color pulses along the plasma filament and the electron screening due to plasma density, various theoretical models have been proposed in 2006 [3], 2012 [8, 11] and 2014 [12]. A general consensus among the models is that higher frequencies are distributed in lower aperture angle cones [8, 11, 12]. In 2018, Ushakov *et al.* studied the THz beam profile as a function of the pump laser focusing conditions. They found that only low numerical apertures ($>$ 10 mm long filaments, NA $<$ 0.02) support conical emission [13]. This is contrary to the measurements in ref. [3], where a focusing lens with a 50 mm focal length showed a conical emission, whereas a 500 mm focal length exhibited a clear uni-modal one. Due to the lack of consensus on the emission profile characteristics in the community, more careful work is required.

Various experimental apparatus have been used to study the spatial transverse distribution of THz radiation from two-color air plasmas. Most works have been performed with detectors such as pyroelectric sensors or Golay cells [8–12]. The main disadvantage of these incoherent thermal detectors is their ultra-broadband spectral response. Even with the use of additional frequency filters such as silicon or high-density polyethylene (HDPE), it is always a challenge to limit the spectral response to the 0.1-5 THz region of interest. Very few papers were focused on characterizing the THz emission by using electro-optic sampling [3, 13]. In all cases, point-by-point measurement or line scanning was used to reconstruct the spectrally-resolved 2D transverse THz beam distribution.

Another important experimental aspect in any two-color air plasma setup concerns the necessity to block the remaining powerful forward-propagating laser light emerging from the plasma filament, whose fluence can exceed 1 mJ/cm^2. Most experiments performed by Ti:Sapphire lasers use a semiconductor silicon wafer owing to its high resistance and low THz absorption. However, as previously noted in a few papers [10, 12], the energy of the photon of the laser pump light is significantly above the 1.24 eV bandgap of silicon, meaning that the laser pulse can easily excite photocarriers in the silicon wafer. This induces a large increase of the silicon reflectivity near the THz beam center,

decaying with the nanosecond lifetime of the excited carriers. The role of photoinduced losses in the silicon wafer has been studied using a Golay cell placed on a 2D raster-scan stage [10]. For long distances between the plasma and the silicon wafer ($>$ 200 mm), the conical THz emission exhibits an additional central peak. The authors concluded that this on-axis emission feature suggests a second emission mechanism in the plasma.

In this letter, similarly to ref. [13], we investigate the frequency-resolved angular distribution of the THz emission, in the 0.2-3 THz range, generated by a Ti:Sapphire two-color laser-induced air plasma filaments. For that purpose, we used a real-time 2D electro-optic coherent detection scheme providing a direct characterization of the transverse THz electric field distribution. Similar to most previous works, the THz diverging emission has been measured just after the plasma to avoid any perturbations from additional optics such off-axis parabolic mirrors or lenses. We paid a special attention to the filter used to block the forward-propagating laser light after the plasma filament. We will discuss the influence of this filter on the THz beam propagation by comparing a small bandgap silicon filter with a ceramic filter. This latter presents a large bandgap ($>$ 6 eV), high ablation resistance and decent THz transmission (60 % at 1 THz, 1 mm filter thickness) [14].

The experiment is outlined in Fig. 1. An infrared laser pulse (50 fs, 800 nm, 2 mJ, R = 5 mm beam waist, 1 kHz repetition rate) is focused in air by a plano-convex lens L1 with a focal length f ranging from 150 mm to 430 mm. After passing through a BBO crystal for second harmonic generation, the resulting intense two-color laser pulse can produce a filament in air whose length depends on the numerical aperture NA defined as NA = $\sin(\arctan(R/f))$. Then, an intense THz pulse is emitted from the plasma filament. Two different detection schemes have been used to characterize the THz emission. First, we used an incoherent detection composed of a Golay cell (GC) (Tydex GC-1P) connected to a lock-in amplifier, an entrance aperture (AP) with 3 mm diameter positioned at 150 mm from the plasma center and a combination of silicon (SF) and ceramic (CF) filters (Fig. 1). The silicon wafer (high resistivity float zone silicon, thickness 1 mm) and the ceramic filter (96% Al_2O_3, thickness 1 mm) were provided by Tydex and CSC Ltd, respectively. Two experimental configurations were considered: while the position of the silicon filter is fixed, the ceramic filter can be either 50 mm before (CF(A)) or 5 mm behind (CF(B)) the latter. For both filtering configurations, the filters and the Golay cell are placed on a rotation stage in order to measure the amplitude of the THz transverse emission profile as a function of the half-opening angle (HOA), as defined in Fig. 1.

The second detection system consists in 2D electro-optic sampling (2DEOS) to measure the time-dependent spatial distribution of the THz electric field [15]. The THz beam is sent into a large aperture (20 mm diameter), 1 mm thick, $\langle 110 \rangle$ ZnTe crystal (Fig. 2), positioned 60 mm behind the center of the plasma filament. By 2DEOS with a time-delayed femtosecond laser probe pulse, we are able to transfer the THz electric field distribution onto the spatial profile of the laser probe beam, which is detected by a 256 $\times$ 256 pixels CMOS camera. For a given time delay between the THz and the probe pulses, the system is able to provide a 2D image at 800 nm, corresponding to the distribution of the THz electric field. This image can be obtained with a 500 Hz acquisition rate thanks to the synchronization with the laser repetition rate and a dynamic subtraction method [16]. To analyze the data, each pixel was Fourier-transformed along its time delay-axis to provide the frequency-resolved 2D THz amplitude and phase distribution of the THz electric field from 0.2 to 3 THz, limited by the spectral bandwidth of the ZnTe crystal and the filters. It is important to note that all data were corrected to account for the Gaussian transverse profile of the large probe laser beam (10 mm beam radius, measured at $1/e^2$), which automatically decreases the THz amplitude out of the center of the beam. Again, two experimental configurations were considered. The silicon filter is placed 50 mm after the center of the plasma filament whereas the ceramic filter can be either 10 mm before (CF(A)) or 5 mm behind (CF(B)) the silicon one.

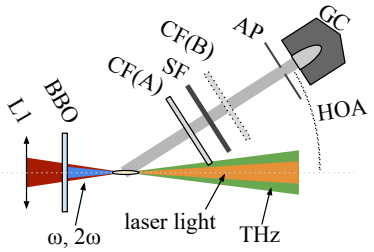

Fig. 1. Incoherent 1D THz detection with a Golay cell. L1: plano-convex lens with focal length f. CF: ceramic filter, SF: silicon filter, AP: aperture, GC: Golay cell. HOA: half-opening angle. Two configurations were relevant: alumina first CF(A) or silicon first CF(B).

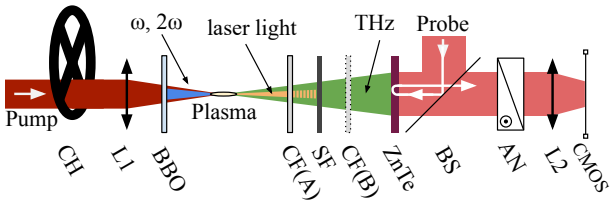

Fig. 2. Coherent 2D electro-optic sampling setup. CH: optical chopper for dynamic subtraction, L1: plano-convex lens with focal length f. CF: ceramic filter, SF: silicon filter, BS: beam-splitter, AN: analyzer, L2: objective lens f = 50 mm. Two configurations were relevant: alumina first (CF(A)) or silicon first (CF(B)).

For a f = 300 mm focusing lens L1 (NA = 0.0167, 5 mm filament length), Fig. 3 represents the incoherent THz emission profile as a function of the HOA. In the silicon first configuration CF(B), with a 2 mJ pump laser light illuminating the silicon wafer, we estimated that the laser light fluence on the silicon wafer is

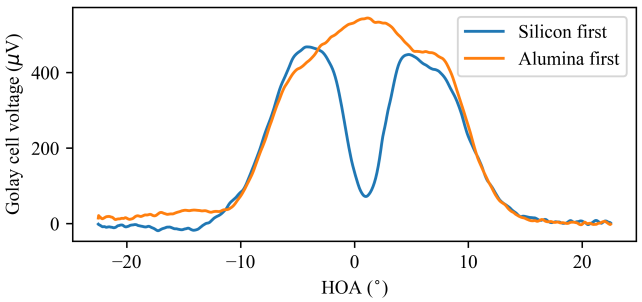

Fig. 3. Incoherent detection of the THz emission profile for the two experimental configurations: alumina first CF(A) and silicon first CF(B).

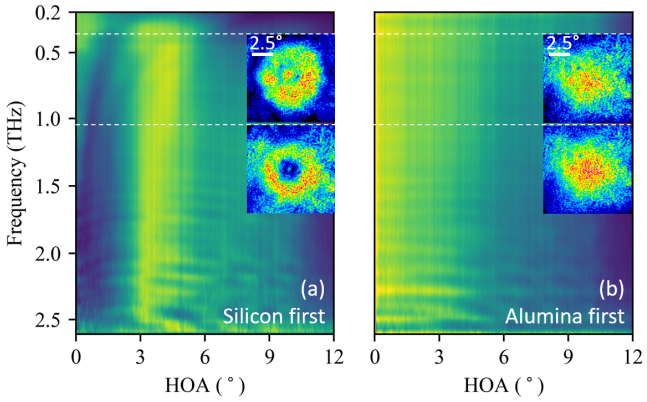

Fig. 4. 2DEOS evolution of THz amplitude as a function of frequency and HOA, in the case of silicon first CF(B) (left) and alumina first CF(A) (right). Yellow color indicates higher THz amplitude. Insets: 2D spatial distributions of the THz electric field at 0.37 THz and 1.05 THz.

as high as 4 mJ/cm^2. The data plot shows a distinct depression in the central part of the emission. The resulting conical THz emission has a HOA of 5° to 6°, in agreement with previous results [8, 12]. We can also notice that the hole diameter is in the same range as the size of the laser pump light illuminating the silicon wafer. The situation is different for the alumina first case CF(A) where the THz emission is maximum in the center like a Gaussian beam. We conclude that if the silicon filter is the first optical element after the plasma filament, *i.e.* it is shined by both the THz beam and the remaining laser pump light, the transmitted THz beam exhibits a conical emission. A similar result has been obtained using a Si wafer from another company. It is worth noting that, outside the center of the THz beam, both configurations exhibit similar HOA.

As explained previously, the main disadvantage of the incoherent thermal detection obtained with the Golay cell is the incapacity to completely block the high THz frequencies ranging from 10 to 25 THz, even with the use of silicon, alumina and HDPE filters. Therefore, we repeated the same measurement with the 2DEOS imaging system, which also allows the direct time-dependent measurement of the 2D THz electric field. Figure 4 represents the evolution of THz amplitude as a function of frequency and HOA, in the case of silicon first CF(B) (left) and alumina first CF(A) (right). Here, HOA $= \arctan(r/60)$, where r is the distance in mm between the center of the THz beam and the measured spot. The measurements have been performed with the $f = 300$ mm focusing lens L1 (NA $= 0.0167$). For a given distance from the center of the beam, we averaged the THz amplitude along the azimuthal angle in order to get the 2D map presented in Fig. 4.

With the silicon filter first CF(B), the central beam hole is evident for frequencies higher than 0.5 THz (Fig. 4, left). The HOA of this central dark region is about 3.5° at 0.5 THz, slightly decreasing below 3.0° at 2.5 THz. The two insets also show the 2D spatial distributions of the THz electric field amplitude, for different frequencies. At 1.05 THz (dotted white line in Fig. 4), the THz beam exhibits a clear conical profile. For frequencies below 0.5 THz (dotted white line at 0.37 THz), a central peak can be observed in the center of the bright ring. We believe that the silicon filter acts as a reflective or absorbing material for THz radiation in this region due to the presence of photo-carriers induced by the remaining pump laser light thus leading to the diffraction-like pattern observed below 0.5 THz. Let us note that the central depression has been observed down to the detection sensitivity limit, corresponding to a laser pump pulse energy of 250 µJ (data not shown). However, this still corresponds to an incident laser light fluence of nearly 0.4 mJ/cm^2 on the silicon wafer, which is sufficient for photo-carriers excitation. We also consider that the uni-modal THz emission below 0.5 THz cannot be attributed to the plasma absorption since it is not observed in the alumina first case, in contradiction with ref. [13].

For the alumina first case CF(A), as previously observed with the incoherent detection, for all frequencies, no central hole is observed in the THz emission (Fig. 4, right). The THz emission exhibits a Gaussian-like profile with a slight decreasing FWMH if the frequency increases. This result is also shown in the two insets representing the 2D spatial distributions of the THz electric field amplitude at 0.37 THz and 1.05 THz. The insets highlight here the clear Gaussian-like THz profiles.

To test our assumption of photo-carriers excitation in silicon filter induced by the laser light, we conducted a complementary experiment. With the 2DEOS setup and with the alumina filter first, we have enough space to irradiate the silicon filter with an oblique incidence 800 nm laser pulse (10 µJ, 5 mm beam waist giving a light fluence of 10 µJ/cm^2), with a time delay τ with respect to the THz pulse peak controlled by a delay line. This additional laser beam overlaps the center of the THz beam at the silicon filter position with a light fluence which is 400 times smaller than the experiments depicted in, Figs. 3 and 4. For various time delays τ between the THz pulse and the oblique infrared pulse, Fig. 5 shows the evolution of the 2D THz electric field sampled at its maximum. The red color indicates a positive electric field and the blue color a negative one (the white color reflects the absence of THz signal), confirming the divergence of the THz beam emerging from the plasma filament. For $\tau \leq 0$, the oblique laser pulse interacts with the silicon filter after the arrival of the THz pulse and we observe a typical divergent THz electric field distribution with a maximum amplitude in the center. Then, for positive values of τ, we clearly observe the time-dependent photo-excitation of the silicon wafer by the laser pulse, with a right to left curtain effect due to the oblique incidence between the THz and laser beams. As a result, for $\tau \geq 4.00$ ps, we observe a white central disk indicating the absence of THz signal in this area. This confirm our assumption

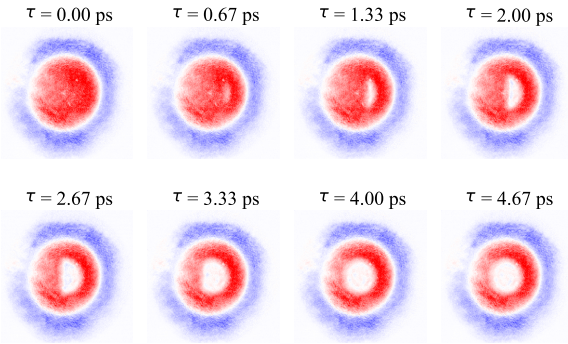

Fig. 5. Evolution of the 2D THz electric field as a function of time delays τ between the THz pulse and the additional oblique infrared laser pulse. Blue, white and red is for negative, zero and positive THz electric field, respectively. White ring angular diameter is 4.7°. The experimental configuration corresponds to alumina filter first CF(A).

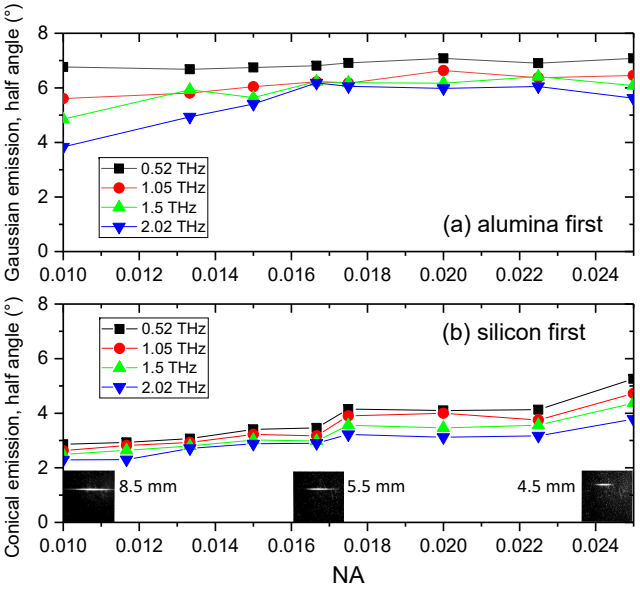

Fig. 6. (a) Alumina first. Evolution of the half angle of the Gaussian-like THz beam as a function of the numerical aperture NA. (b) Silicon first. Evolution of the half angle of the conical THz beam as a function of the numerical aperture NA. Insets: pictures of plasma filaments and filament lengths, image sizes are 10×10 mm^2.

of photo-carriers excitation in the silicon filter. The central THz beam is fully reflected (or absorbed) by the silicon filter and exhibit a conical distribution which can persist much longer than the laser pulse duration due to the nanosecond charge carrier lifetime in silicon.

Finally, we investigated the dependence of the far-field THz beam with respect to the laser focusing conditions. With the 2DEOS detection, we measured the frequency-resolved THz electric field as a function of the numerical aperture NA, from NA $= 0.01$ ($f = 500$ mm, 8.5 mm plasma length) to NA $= 0.025$ ($f = 200$ mm, 4.5 mm plasma length), as shown in Fig. 6. As previously explained, data were corrected to take into account the Gaussian transverse profile of the probe laser beam. We first consider the case of alumina filter first (Fig. 6(a)). The data points have been obtained by fitting the THz beam profile with a Gaussian function. For a given NA, the THz half emission angle (corresponding to the half angular width of the beam at half maximum amplitude) decreases as the THz frequency increases, as previously observed in refs. [8, 11, 12]. For a given frequency, it is worth noting that the THz half emission angle barely increases (about 1°) as NA increases. It means that the THz far-field distribution, in the 0.2-3 THz spectral range and for this NA range, is not strongly governed by the laser focusing conditions. To our knowledge, this has never been observed previously. Uni-modal angular distribution had previously been observed in the 0.3–3 THz range only for moderate focusing by Ushakov *et al.* (NA > 0.035) [13]. For long focal lengths as in Fig. 6(a) (NA < 0.02), only conical emission were reported so far. Especially, Ushakov *et al.* concluded that decreasing NA up to 0.02 is important to observe a ring-structure, which is in contradiction with our experiment. We can also notice that these authors observed a strong on-axis peak for NA $=$ 0.02, superimposed on the conical emission, which was not reproduced by their simulations. We then consider the case of silicon filter first (Fig. 6(b)). The graph shows the evolution of the half angle of the far-field conical THz beam as a function of NA. As previously observed, the conical angle increases if the frequency decreases or if NA increases [8, 11, 12]. This is consistent with the observation that if NA increases (tighter laser focusing), then the pump laser light can excite photo-carriers onto a larger area of the silicon wafer, resulting in a larger conical angle THz emission.

To conclude, we have shown that the silicon filter used to block the remaining laser light behind the Ti:Sapphire two-color air plasma filament has a strong influence on the existence of the far-field conical THz distribution. We concluded that this conical beam is due to photo-excited charge carriers in the silicon wafer. If the laser light was sufficiently scattered or absorbed by a preceding large bandgap alumina filter, we observed a TEM_{00} Gaussian-like THz distribution from 0.2 to 3 THz, which was not strongly governed by the laser focusing conditions under our experimental conditions. These measurements call for further detailed simulations of the THz emission from a two-color plasma, which will require consideration of the full spatio-temporal wave propagation in the plasma.

Funding. The author acknowledges funding from the Danish Independent Research Fund grant (DFF-6111-00119, 2016) and the LAPHIA Student mobility grant 2019. The Conseil Régional Nouvelle Aquitaine and FEDER are also thanked for funding the equipments of the COLA platform at LOMA.

REFERENCES

1. D. J. Cook and R. M. Hochstrasser, Opt. Lett. **25**, 1210 (2000).
2. M. Kress, T. Löffler, S. Eden, M. Thomson, and H. G. Roskos, Opt. Lett. **29**, 1120 (2004).
3. H. Zhong, N. Karpowicz, and X.-C. Zhang, Appl. Phys. Lett. **88**, 261103 (2006).
4. H. Roskos, M. Thomson, M. Kreß, and T. Löffler, Laser & Photonics Rev. **1**, 349 (2007).
5. T. Oh, y. s. You, and K. Kim, Opt. express **20**, 19778 (2012).
6. J. Zhao, W. Liu, S. Li, D. Lu, Y. Zhang, Y. Peng, Y. Zhu, and S. Zhuang, Photon. Res. **6**, 296 (2018).
7. K.-Y. Kim, J. H. Glownia, A. J. Taylor, and G. Rodriguez, IEEE J. Quantum Electron. **48**, 797 (2012).
8. Y. S. You, T. I. Oh, and K. Y. Kim, Phys. Rev. Lett. **109** (2012).
9. P. Klarskov, A. C. Strikwerda, K. Iwaszczuk, and P. U. Jepsen, New J. Phys. **15**, 075012 (2013).
10. V. Blank, M. D. Thomson, and H. G. Roskos, New J. Phys. **15**, 075023 (2013).
11. A. V. Borodin, M. N. Esaulkov, I. I. Kuritsyn, I. A. Kotelnikov, and A. P. Shkurinov, JOSA B **29**, 1911 (2012).
12. A. Gorodetsky, A. D. Koulouklidis, M. Massaouti, and S. Tzortzakis, Phys. Rev. A **89**, 033838 (2014).
13. A. A. Ushakov, P. A. Chizhov, V. A. Andreeva, N. A. Panov, D. E. Shipilo, M. Matoba, N. Nemoto, N. Kanda, K. Konishi, V. V. Bukin, M. Kuwata-Gonokami, O. G. Kosareva, S. V. Garnov, and A. B. Savel'ev, Opt. Express **26**, 18202 (2018).
14. K. Z. Rajab, M. Naftaly, E. H. Linfield, J. C. Nino, D. Arenas, D. Tanner, R. Mittra, and M. Lanagan, J. Microelectron. Electron. Packag. **5**, 2 (2008).
15. M. Brossard, H. Cahyadi, M. Perrin, J. Degert, E. Freysz, T. Yasui, and E. Abraham, IEEE Transactions on Terahertz Sci. Technol. **7**, 741 (2017).
16. Z. Jiang, X. G. Xu, and X.-C. Zhang, Appl. Opt. **39**, 2982 (2000).

FULL REFERENCES

1. D. J. Cook and R. M. Hochstrasser, "Intense terahertz pulses by four-wave rectification in air," Opt. Lett. **25**, 1210 (2000).
2. K.-Y. Kim, J. H. Glownia, A. J. Taylor, and G. Rodriguez, "High-Power Broadband Terahertz Generation via Two-Color Photoionization in Gases," IEEE J. Quantum Electron. **48**, 797–805 (2012).
3. M. Thomson, V. Blank, and H. G. Roskos, "Terahertz white-light pulses from an air plasma photo-induced by incommensurate two-color optical fields," Opt. Express **18**, 23173–23183 (2010).
4. H. Zhong, N. Karpowicz, and X.-C. Zhang, "Terahertz emission profile from laser-induced air plasma," Appl. Phys. Lett. **88**, 261103 (2006).
5. P. Klarskov, A. C. Strikwerda, K. Iwaszczuk, and P. U. Jepsen, "Experimental three-dimensional beam profiling and modeling of a terahertz beam generated from a two-color air plasma," New J. Phys. **15**, 075012 (2013).
6. V. Blank, M. D. Thomson, and H. G. Roskos, "Spatio-spectral characteristics of ultra-broadband THz emission from two-colour photoexcited gas plasmas and their impact for nonlinear spectroscopy," New J. Phys. **15**, 075023 (2013).
7. Y. S. You, T. I. Oh, and K. Y. Kim, "Off-Axis Phase-Matched Terahertz Emission from Two-Color Laser-Induced Plasma Filaments," Phys. Rev. Lett. **109** (2012).
8. A. V. Borodin, M. N. Esaulkov, I. I. Kuritsyn, I. A. Kotelnikov, and A. P. Shkurinov, "On the role of photoionization in generation of terahertz radiation in the plasma of optical breakdown," JOSA B **29**, 1911–1919 (2012).
9. A. Gorodetsky, A. D. Koulouklidis, M. Massaouti, and S. Tzortzakis, "Physics of the conical broadband terahertz emission from two-color laser-induced plasma filaments," Phys. Rev. A **89** (2014).
10. A. A. Ushakov, P. A. Chizhov, V. A. Andreeva, N. A. Panov, D. E. Shipilo, M. Matoba, N. Nemoto, N. Kanda, K. Konishi, V. V. Bukin, M. Kuwata-Gonokami, O. G. Kosareva, S. V. Garnov, and A. B. Savel'ev, "Ring and unimodal angular-frequency distribution of THz emission from two-color femtosecond plasma spark," Opt. Express **26**, 18202 (2018).
11. J. Jones, C. McEnnis, Y. Dikmelik, J. Spicer, D. Drewry, and M. Leahy-Hoppa, "Terahertz Time-Domain Spectroscopy of Aluminum Oxide for Thermal Protection Applications," in *48th AIAA/ASME/ASCE/AHS/ASC Structures, Structural Dynamics, and Materials Conference,* (American Institute of Aeronautics and Astronautics, Honolulu, Hawaii, 2007).
12. K. Z. Rajab, M. Naftaly, E. H. Linfield, J. C. Nino, D. Arenas, D. Tanner, R. Mittra, and M. Lanagan, "Broadband Dielectric Characterization of Aluminum Oxide (Al_2O_3)," J. Microelectron. Electron. Packag. **5**, 2–7 (2008).
13. M. Brossard, H. Cahyadi, M. Perrin, J. Degert, E. Freysz, T. Yasui, and E. Abraham, "Direct Wavefront Measurement of Terahertz Pulses Using Two-Dimensional Electro-Optic Imaging," IEEE Transactions on Terahertz Sci. Technol. **7**, 741–746 (2017).

FULL REFERENCES

1. D. J. Cook and R. M. Hochstrasser, "Intense terahertz pulses by four-wave rectification in air," Opt. Lett. **25**, 1210 (2000).
2. K.-Y. Kim, J. H. Glownia, A. J. Taylor, and G. Rodriguez, "High-Power Broadband Terahertz Generation via Two-Color Photoionization in Gases," IEEE J. Quantum Electron. **48**, 797–805 (2012).
3. M. Thomson, V. Blank, and H. G. Roskos, "Terahertz white-light pulses from an air plasma photo-induced by incommensurate two-color optical fields," Opt. Express **18**, 23173–23183 (2010).
4. H. Zhong, N. Karpowicz, and X.-C. Zhang, "Terahertz emission profile from laser-induced air plasma," Appl. Phys. Lett. **88**, 261103 (2006).
5. P. Klarskov, A. C. Strikwerda, K. Iwaszczuk, and P. U. Jepsen, "Experimental three-dimensional beam profiling and modeling of a terahertz beam generated from a two-color air plasma," New J. Phys. **15**, 075012 (2013).
6. V. Blank, M. D. Thomson, and H. G. Roskos, "Spatio-spectral characteristics of ultra-broadband THz emission from two-colour photoexcited gas plasmas and their impact for nonlinear spectroscopy," New J. Phys. **15**, 075023 (2013).
7. Y. S. You, T. I. Oh, and K. Y. Kim, "Off-Axis Phase-Matched Terahertz Emission from Two-Color Laser-Induced Plasma Filaments," Phys. Rev. Lett. **109** (2012).
8. A. V. Borodin, M. N. Esaulkov, I. I. Kuritsyn, I. A. Kotelnikov, and A. P. Shkurinov, "On the role of photoionization in generation of terahertz radiation in the plasma of optical breakdown," JOSA B **29**, 1911–1919 (2012).
9. A. Gorodetsky, A. D. Koulouklidis, M. Massaouti, and S. Tzortzakis, "Physics of the conical broadband terahertz emission from two-color laser-induced plasma filaments," Phys. Rev. A **89** (2014).
10. A. A. Ushakov, P. A. Chizhov, V. A. Andreeva, N. A. Panov, D. E. Shipilo, M. Matoba, N. Nemoto, N. Kanda, K. Konishi, V. V. Bukin, M. Kuwata-Gonokami, O. G. Kosareva, S. V. Garnov, and A. B. Savel'ev, "Ring and unimodal angular-frequency distribution of THz emission from two-color femtosecond plasma spark," Opt. Express **26**, 18202 (2018).
11. J. Jones, C. McEnnis, Y. Dikmelik, J. Spicer, D. Drewry, and M. Leahy-Hoppa, "Terahertz Time-Domain Spectroscopy of Aluminum Oxide for Thermal Protection Applications," in *48th AIAA/ASME/ASCE/AHS/ASC Structures, Structural Dynamics, and Materials Conference,* (American Institute of Aeronautics and Astronautics, Honolulu, Hawaii, 2007).
12. K. Z. Rajab, M. Naftaly, E. H. Linfield, J. C. Nino, D. Arenas, D. Tanner, R. Mittra, and M. Lanagan, "Broadband Dielectric Characterization of Aluminum Oxide (Al_2O_3)," J. Microelectron. Electron. Packag. **5**, 2–7 (2008).
13. M. Brossard, H. Cahyadi, M. Perrin, J. Degert, E. Freysz, T. Yasui, and E. Abraham, "Direct Wavefront Measurement of Terahertz Pulses Using Two-Dimensional Electro-Optic Imaging," IEEE Transactions on Terahertz Sci. Technol. **7**, 741–746 (2017).